J. Fluid Mech. (2008), *vol.* 605, *pp.* 253–262.
doi:10.1017/S0022112008001626 Printed in the United Kingdom

Flow over a thin circular disk at low to moderate Reynolds numbers

A. R. SHENOY AND C. KLEINSTREUER†

Department of Mechanical and Aerospace Engineering, North Carolina State University, Raleigh, NC 27695-7910, USA

(Received 23 October 2007 and in revised form 14 March 2008)

Computation of viscous flow over a circular disk of aspect ratio 10 (thickness/diameter) in the Reynolds number (Re) range of 10 to 300 was performed. The following flow regimes were observed: (I) steady axisymmetric flow when $Re < 135$, with the presence of a toroidal vortex behind the disk; (II) regular bifurcation with loss of azimuthal symmetry but with planar symmetry and a double-threaded wake, for $135 \leqslant Re < 155$; (III) three-dimensional flow with periodic shedding of double-sided hairpin-shaped vortex structures and periodic motion of the separation region for $155 \leqslant Re < 172$; (IV) regular shedding of double-sided hairpin-shaped vortex structures with planar and spatio-temporal symmetry for $172 \leqslant Re < 280$; (V) periodic three-dimensional flow with irregular rotation of the separation region when $Re = 280$–300. This transition process for the disk differs from that for the sphere as we observe a loss of the symmetry plane in Regime III due to a twisting motion of the axial vorticity strands in the wake of the disk. The periodic flow was characterized by double-sided hairpin structures, unlike the one-sided vortex loops observed for the sphere. This resulted in the drag coefficient oscillating at twice the frequency of the axial velocity. In Regime IV, the vortex loops were shed from diametrically opposite locations and with equal strength, resulting in the lift coefficient oscillating symmetrically about a zero mean. These results imply the presence of spatio-temporal symmetry.

1. Introduction

Steady flow over a three-dimensional bluff body, beyond a critical Reynolds number, bifurcates into a periodic oscillatory flow with vortex shedding. The flow typically exhibits a dominant disturbance mode, exemplified by the spatial wavenumbers $m = 0, \pm 1, \pm 2, \ldots$. Periodic shedding of hairpin-shaped vortices, with the same orientation, forming a ladder-like chain of overlapping loops, have been observed for a sphere (Achenbach 1974; Magarvey & Bishop 1961) and a disk (Marshall & Stanton 1930). A linear stability analysis (LSA) by Natarajan & Acrivos (1993) for flow over a sphere and a disk revealed that the onset of unsteadiness was a two-step process, namely regular and Hopf bifurcations, due to a dominant first helical mode ($m = \pm 1$). The regular bifurcation is identified by a loss of azimuthal symmetry and a double-threaded wake (Magarvey & Bishop 1961) at a transition Reynolds number $Re_1 = 210$. A Hopf bifurcation leads to periodic vortex shedding behind a bluff body at Reynolds number $Re_2 = 270$. The vortex structure in the sphere wake consists of

† Author to whom correspondence should be addressed: ck@eos.ncsu.edu.

single-sided vortex loops, leading the axial velocity in the wake to oscillate at the same frequency as the axial drag coefficient (C_D) and a non-zero mean lift coefficient (C_L). Both the regular and Hopf bifurcations have been shown to be supercritical (Thompson, Leweke & Provansal 2001), for a sphere by determining coefficients of the Landau model. With increasing Reynolds number, the vortex shedding location changes irregularly along the azimuthal direction from cycle to cycle (Sakamoto & Haniu 1990), leading to a fully three-dimensional flow at $Re_3 = 420$. However, there is planar symmetry in the range $Re_1 \leqslant Re < Re_3$.

Numerical investigations (Johnson & Patel 1999; Mittal 1999; Tomboulides & Orszag 2000), have successfully identified these different regimes for a sphere, but a similar study for the disk has not been conducted. Secondary vortex structure formed around the legs of the shed hairpin vortex was reported by Johnson & Patel (1999) and later verified by Brücker (2001) through a spatio-temporal reconstruction of the wake. These structures are not shed from the recirculating region but formed due to the interaction of the shed hairpin structure and the wake/outer flow. The aspect ratio (χ = thickness/diameter) of the disk could play a significant role in determining the transition process and vortex structure in the wake. For example, numerical simulations by Fernandes *et al.* (2007) found the transition Reynolds numbers to be a function of the disk aspect ratio, $Re_1 = 116.5(1 + \chi^{-1})$ and $Re_2 = 125.6(1 + \chi^{-1})$. Their study did not address effects of the disk aspect ratio on the vortex structure in the wake and was limited to $Re < Re_3$. Recent results by Fabre, Auguste & Magnaudet (2007) have indicated that the flow transition for an infinitely thin disk, in contrast to the sphere, is a three-step process: the regular bifurcation is followed by two successive bifurcations. The first bifurcation leads to fully three-dimensional flow with periodic vortex shedding and a loss of the symmetry plane. In the second, the flow remains periodic and the symmetry plane is recovered. These results indicate that a detailed study of the transition process for the disk and the associated vortex structure is required.

In this paper, flow past a circular disk of aspect ratio 10, for a Reynolds number range of 10 to 300, has been numerically analysed. The different flow regimes, oscillation frequencies and vortex structures are identified.

2. Numerical formulation

Steady and transient incompressible flow fields around a circular disk of diameter D and aspect ratio $\chi = 10$ has been computed and visualized. The computational domain with a circular cross-section of diameter $D_c = 12D$ was situated along the z-direction, see figure 1, with the centre of the disk located on the z-axis and its upstream surface in the (x, y)-plane. The domain extended $z_d = 15D$ downstream and $z_u = 2.5D$ upstream of the disk. A hexahedral mesh with an O-grid topology consisting of 59 556 elements and 61 836 nodes was generated using the commercial grid generation software ICEM-CFD (ANSYS Inc., 2007). A refined mesh, as shown in figure 1, was used close to the surface of the disk in both axial and radial directions to accurately capture steep gradients. The numerical solution of the incompressible Navier–Stokes equations was carried out using the finite-volume-based commercial code CFX-10.0 (ANSYS Inc., 2005). This numerical program relies on an unstructured body-fitted grid with collocated pressure and velocity nodes. The numerical algorithm is based on the SIMPLEC methodology with the Rhie-Chow interpolation scheme to prevent the decoupling of the pressure and velocity fields, typically observed on collocated grids. A robust second-order implicit backward Euler scheme was used

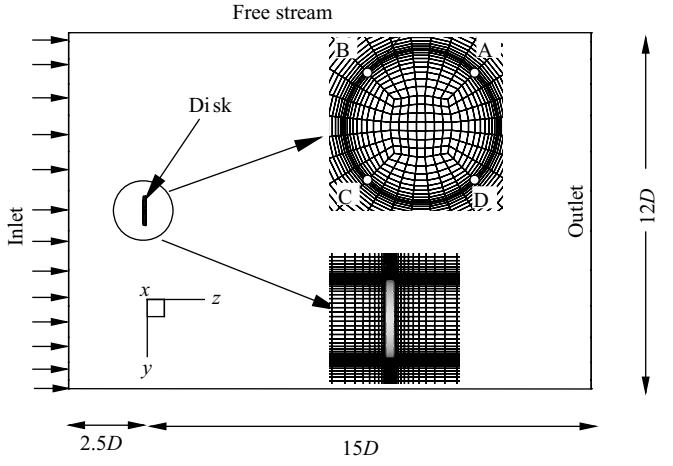

FIGURE 1. Computational domain and grid structure near the disk surface.

for transient simulations. The advection terms were evaluated using a high-resolution scheme with a blending factor (Barth & Jespersen 1989). A fixed time step gave approximately 100 points in one period of the dominant frequency with $CFL < 1$. Uniform velocity and pressure boundary conditions were prescribed at the inlet and outlet, respectively. Free and no-slip boundary conditions were applied to the free stream and disk surface, respectively. For unsteady flow, the history of axial velocity variations was recorded at $z = 0.2D$ (close to the disk) and at $z = 5D$ (in the wake). At each axial location, the velocity was sampled at four points (A, B, C, D) separated by 90°, as shown in figure 1. For proper identification of the vortical regions, the method proposed by Jeong & Hussain (1995) (the so-called λ_2-scheme) was employed.

To determine the effect, if any, of the domain size on the results, a larger domain ($D_c = 24D, z_u = 5D, z_d = 30D$) was also evaluated. A comparison of the drag coefficient (C_D) computed from the large and small domains had a maximum variation of 2% in the Reynolds number range of 10–100. The grid independence of the solution was verified using a fine mesh with 242 066 elements and 247 716 nodes for both steady and transient computations. In figure 2(*a*), the computed axial drag coefficient (C_D) for both coarse and fine meshes is compared with experimental data (Ross & Willmarth 1971) for $Re = 10$–100. The length of the wake computed for coarse and fine grids is also compared in figure 2(*a*), but no experimental results for wake length are currently available for a disk. In figure 2(*b*), the lift coefficient (C_L) for the disk at $Re = 180$ is compared for the coarse mesh, fine mesh and the larger domain. The results from the nominal mesh were deemed grid independent and the domain size was found to have no influence on the result.

3. Results

The overall transition process for our disk was found to differ from that of the sphere, as observed by Fabre, Auguste & Magnaudet (2007) for a disk of infinitesimal thickness. The transition was found to be a three-step process with a regular bifurcation followed by two successive bifurcations with periodic vortex shedding. Also, unlike the sphere, the vortex structures in the wake were found to be double sided, namely two oppositely oriented hairpin structures were shed from the recirculating region. At higher Reynolds numbers, the periodic vortex shedding

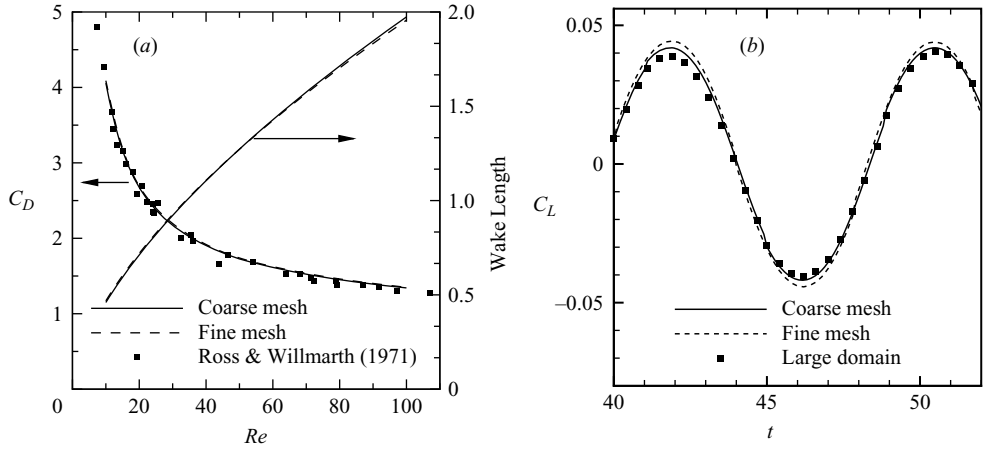

FIGURE 2. (*a*) Comparison of drag coefficient (C_D) and length of the wake for $Re = 10$–100; (*b*) Comparison of periodic variation of the lift coefficient (C_L) for $Re = 180$.

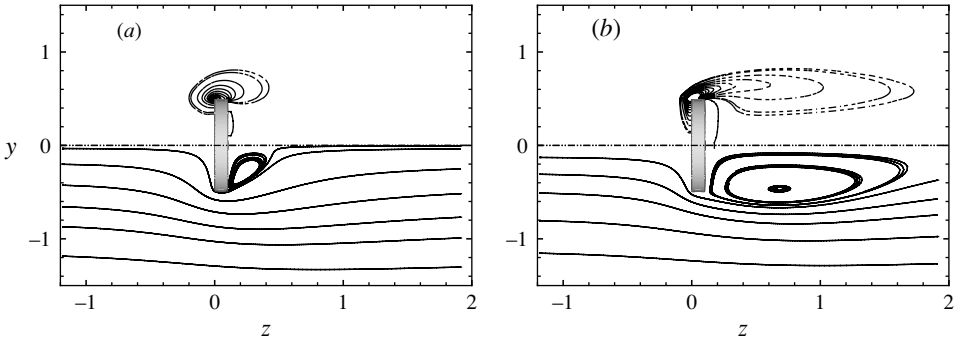

FIGURE 3. Steady axisymmetric flow with azimuthal vorticity (upper half) and streamlines (lower half): (*a*) $Re = 10$; (*b*) $Re = 100$.

persisted, but its location varied irregularly around the circumference. In the following sections these results are discussed in more detail.

3.1. *Steady axisymmetric flow* ($10 < Re < 135$)

In the Reynolds number range of 10–135, the flow was steady, axisymmetric and separated from the leading edge to form a toroidal vortex behind the disk. The size of the recirculating region and the vorticity of the toroidal vortex increased with Reynolds number (see figure 3). At $Re_1 = 135$, the steady axisymmetric flow underwent a regular bifurcation to steady asymmetric flow, as discussed in the next section.

3.2. *Steady asymmetric flow* ($135 \leqslant Re < 155$)

To determine the first critical Reynolds number, transient flow computations were performed for Reynolds numbers greater than 100. Artificial disturbances were introduced through the initial conditions to perturb the flow. The amplitude of the velocity perturbation was varied up to 100% of the free-stream velocity to determine the effect, if any, on the end results. At $Re_1 = 135$, there was a breakdown of azimuthal symmetry leading to a steady asymmetric flow field with a double-threaded wake, i.e. two counter-rotating streamwise (axial) vortices, see figure 4, similar to that

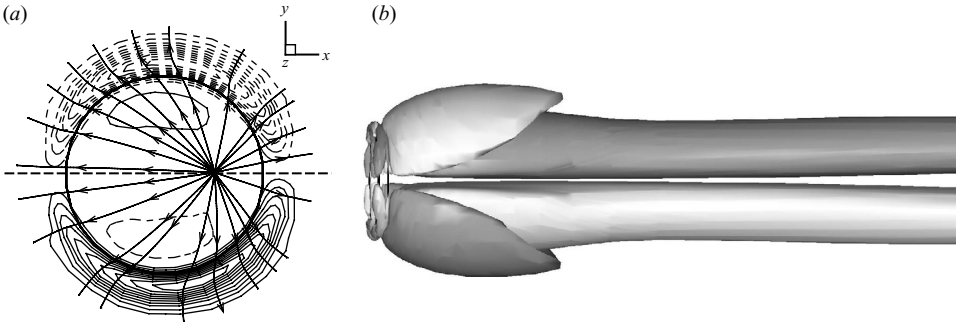

FIGURE 4. Steady non-axisymmetric flow ($Re = 140$) with a symmetry plane (——). (*a*) Axial vorticity and limiting streamlines (shown with arrows). (*b*) Axial vorticity isosurfaces, equal magnitudes of positive and negative vorticity indicated by dark and light surfaces, respectively.

of a sphere (Johnson & Patel 1999; Tomboulides & Orszag 2000; Thompson, Leweke & Provansal 2001). The predicted critical Reynolds number is close to $Re_1 = 128.5$, obtained by Fernandes *et al.* (2007) but higher than the LSA prediction of $Re_1 = 116.5$ owing to the finite thickness of our disk. A symmetry plane, oriented at $\approx 62^\circ$ to the x-axis, was observed. The orientation of the symmetry plane in a numerical simulation is influenced by irregularities in the grid, initial conditions and solver methodology. The results were transformed such that the symmetry plane aligned with the (x, z)-plane. The stagnation point on the downstream surface of the disk is displaced from the centre (see figure 4*a*) signifying loss of axial symmetry. Figure 4 also indicates the presence of an axial vorticity dipole outside the recirculating region, which induces an axial vorticity of opposite sign to originate from the recirculating region, forming strands of vorticity extending far downstream.

3.3. *Three-dimensional periodic flow with regular rotation of the seperation region* ($155 \leqslant Re < 172$)

At $Re_2 = 155$, a Hopf bifurcation was observed with periodic shedding of hairpin-shaped vortices in the wake of the disk. The symmetry plane observed during the regular bifurcation was lost and the flow was fully three-dimensional. The strands of axial vorticity in the wake, observed in the previous regime, were found to coil/kink around each other. Similar 'kinking' of the trailing vortices has been observed for a sphere (Thompson, Leweke & Provansal 2001). Focusing on $Re = 160$, figure 5(*a*) shows the positive and negative strands of axial vorticity twisting around each other near the disk surface and also in the near wake (figure 5*b*). This indicates a loss of the symmetry plane, compared to that observed in figure 4. The axial drag coefficient (C_D) and the angle of lift force (θ) to the x-axis are shown in figure 6(*a*). The direction of the lift force varies periodically at a Strouhal number ($St = fD/U$) of 0.113 between -65° and -10°.

The frequency spectra of the axial velocity (V_z) and C_D are shown in figure 6(*b*), where the velocity oscillates at $St_1 = 0.113$ but the drag coefficient oscillates at $2St_1$. The low-frequency oscillation in C_D could be due to the pumping motion of the recirculating region, namely the $m = 0$ mode (Berger, Scholz & Schumm 1990). The increased periodicity of the drag coefficient is in contrast to that observed for a sphere, where the frequency of oscillation for the axial velocity and the drag coefficient are identical (Johnson & Patel 1999; Tomboulides & Orszag 2000) and matches the vortex shedding frequency measured through flow visualization (Sakamoto & Haniu 1990).

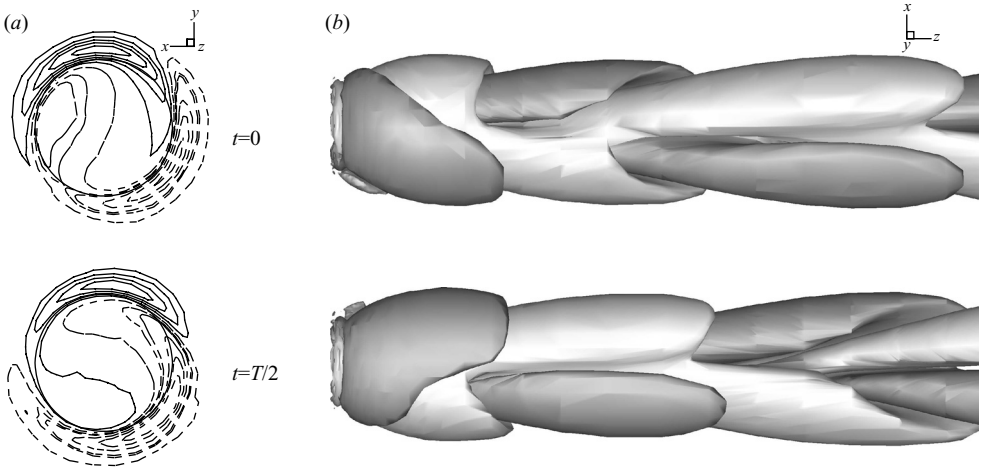

FIGURE 5. Periodic three-dimensional flow ($Re = 160$). (a) Axial vorticity, solid and dashed lines indicate positive and negative values, respectively. (b) Axial vorticity isosurfaces, equal magnitudes of positive and negative vorticity indicated by dark and light surfaces, respectively.

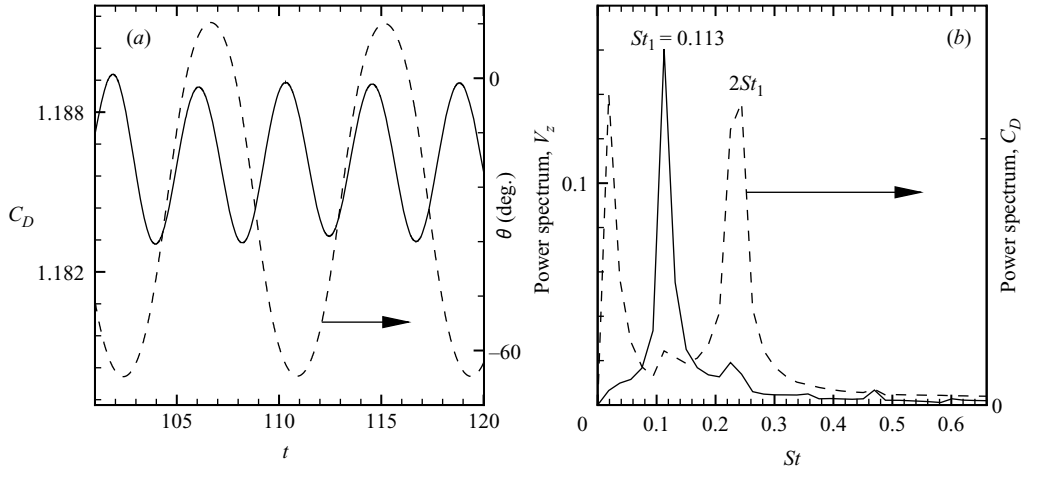

FIGURE 6. Regular vortex shedding ($Re = 160$). (a) Temporal variation of C_D and the orientation of the lift force. (b) Spectral analysis of axial velocity (V_z) and C_D.

Johnson & Patel (1999) do report a smaller peak at twice the fundamental frequency for C_D, but its effect was not significant. These results indicate that unlike the vortex shedding behind a sphere, where one-sided vortex loops are shed, we observe shedding of double-sided hairpin vortices which are shed from the re-circulating region, unlike those observed by Johnson & Patel (1999) due to the interaction of the wake/outer flow. The predicted Strouhal number ($St_1 = 0.113$) compares well with the value of 0.122 reported by Fernandes *et al.* (2007). The predicted critical Reynolds number $Re_2 = 155$ is higher than $Re_2 = 138.16$, determined by Fernandes *et al.* (2007), probably owing to differences in solution algorithm and grid structure. The present result is also higher that that predicted by linear stability analysis (Natarajan & Acrivos 1993) of $Re_2 = 125.6$ owing to the finite-thickness effects. This behaviour of a $\chi = 10$ disk, compared to that of an infinitesimal thickness disk (Fabre, Auguste

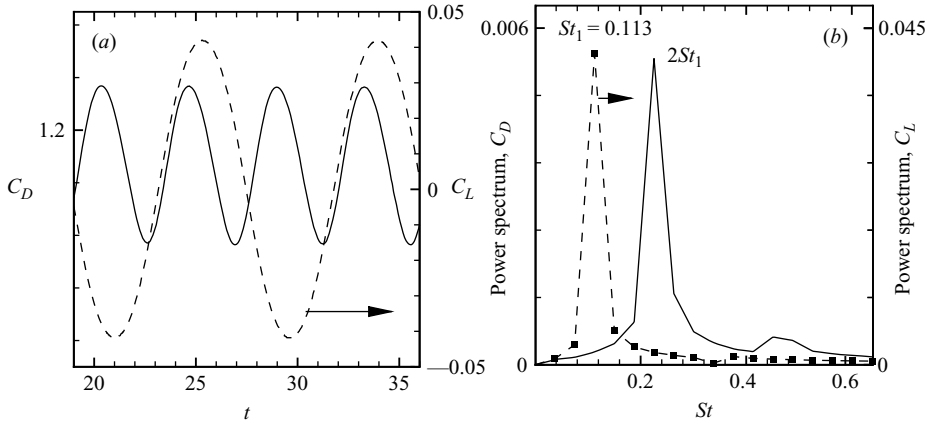

FIGURE 7. Periodic vortex shedding ($Re = 180$). (*a*) Temporal variation of C_D and C_L. (*b*) Spectral analysis of C_L and C_D.

& Magnaudet 2007), indicates that the observed difference in the transition process is not limited to infinitely thin disks. There is probably a critical thickness above which the transition process would exactly match that of the sphere. With increasing Reynolds number, the amplitude of the rotating axial vorticity strands increased and at $Re_2 = 172$ it was observed that the plane of symmetry was restored along with a spatio-temporal symmetry.

3.4. *Unsteady flow with a plane of symmetry* ($172 \leqslant Re < 280$)

At $Re_2 = 172$, planar symmetry was found to emerge with continued periodic shedding of double-sided hairpin-shaped vortices from diametrically opposite locations. Similar planar symmetry has been observed for the sphere (Johnson & Patel 1999; Sakamoto & Haniu 1990; Tomboulides & Orszag 2000). Computational results obtained for $Re = 180$ showed that the lift coefficient (C_L), determined from the lateral force acting along the plane of symmetry, made equal magnitude oscillations about a mean value of zero (see figure 7*a*). This result contrasts with that of a sphere where the lift force was one-sided (Johnson & Patel 1999) and is related to the shedding of symmetric opposite-sided vortex loops. The lift coefficient (C_L) varied periodically at $St_1 = 0.113$ and C_D continued to oscillate at $2St_1$.

The vortex shedding mechanism, visualized using the λ_2-scheme, is shown in figure 8(*a*, *b*). The orientation of the vortex loops indicates a double-sided vortex shedding mode. This is further exemplified in the temporal variation of the azimuthal vorticity contours projected on the symmetry plane depicted in figure 9(*a*) and the axial vorticity contours near the disk surface in figure 9(*b*). The contours are separated by a time interval of half the period of velocity fluctuation. The azimuthal vorticity shown in figure 9(*a*) clearly shows vortices shed alternately from the top and bottom surface of the disk. The axial vorticity contours shown in figure 9(*b*) display a symmetry plane and, in contrast to the vorticity dipole observed in figure 4(*a*), a vorticity quadrupole is observed. The topology of the limiting streamlines on the rear surface of the disk is shown in figure 9(*c*). The streamlines form a node on the symmetry plane that oscillates at a frequency equal to that of the V_z/C_L fluctuation; in contrast, the node behind a sphere is stationary (Johnson & Patel 1999), indicating that the hairpin vortex strongly interacts with the disk surface. These results indicate the presence of a spatio-temporal symmetry, similar to that observed by Barkley & Henderson

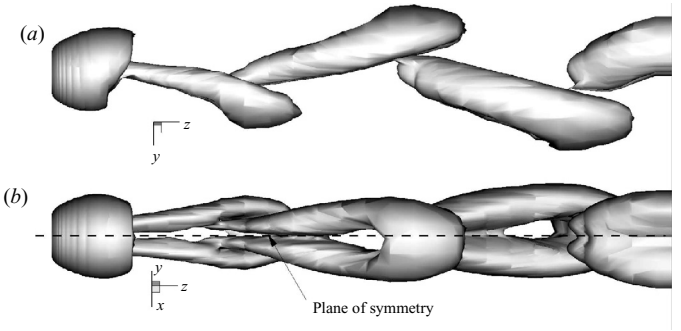

FIGURE 8. Vortical regions (λ_2-scheme) showing regular vortex shedding ($Re = 180$): (a) symmetry plane; (b) perpendicular to the symmetry plane.

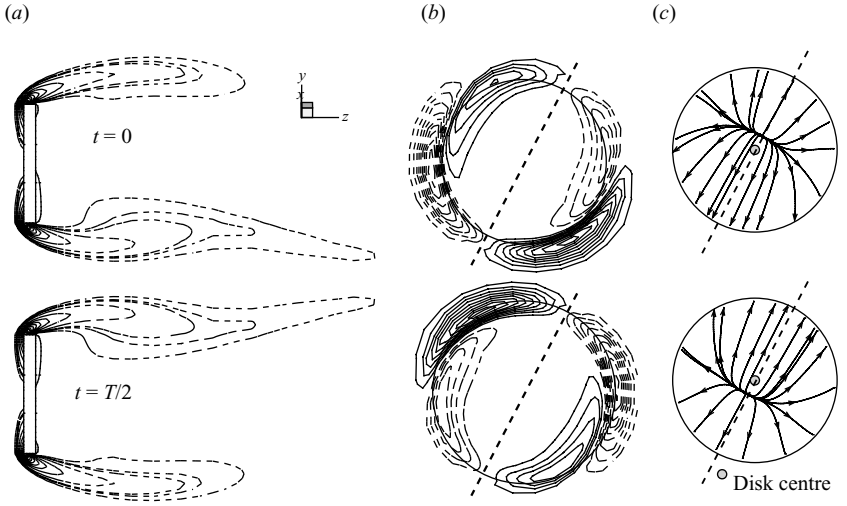

FIGURE 9. Alternate vortex shedding ($Re = 180$). (a) Aximuthal vorticity regions projected on the plane of symmetry. (b) Axial vorticity projected on the (x, y)-plane near the disk surface. (c) Limiting streamlines near the disk surface; solid and dashed lines indicate positive and negative values, respectively.

(1996) during flow transition over a cylinder. This implies that a spatial rotation, in the azimuthal direction, by 180° would match the flow field at a temporal location separated by $T/2$.

3.5. *Unsteady flow with loss of plane of symmetry* ($Re = 300$)

At $Re_3 = 280$, irregular motion of the vortex shedding location led to a loss of planar symmetry. This irregular motion could be a precursor of the helical vortex structures observed at higher Reynolds numbers (Berger, Scholz & Schumm 1990). A similar mechanism for the loss of planar symmetry has been observed for a sphere (Mittal 1999). The computational results obtained for the disk at $Re = 300$ are discussed next. The vortex shedding is visualized in figure 10.

The velocity spectrum (see figure 11a) has a dominant frequency at $St = 0.122$ due to vortex shedding and lower frequency oscillations at $St = 0.041$. The velocity at $z = 0.2D$ also showed a similar influence of the low-frequency oscillation and a higher frequency at $St \approx 0.2$, possibly related to a shear-layer instability near the

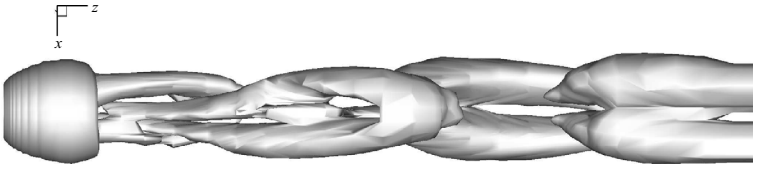

FIGURE 10. Vortical regions (λ_2-scheme) showing irregular vortex shedding ($Re = 300$).

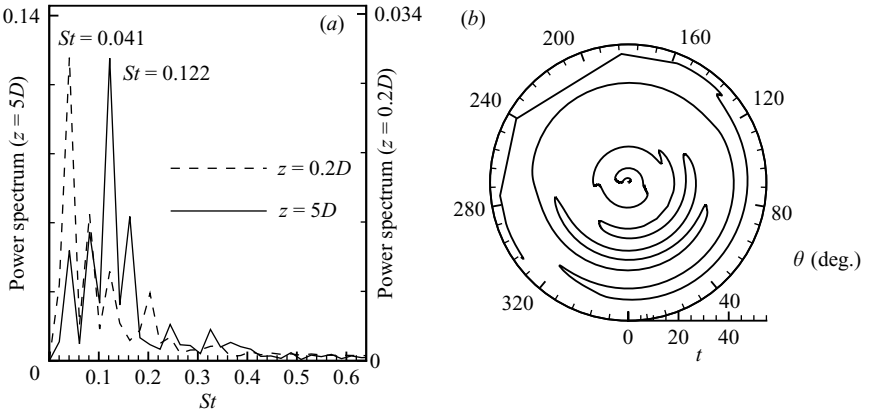

FIGURE 11. Irregular vortex shedding ($Re = 300$). (*a*) Spectral analysis of the axial velocity. (*b*) Temporal evolution of vortex shedding location.

disk. This low-frequency oscillation has been attributed to the irregular motion of the vortex shedding location (Tomboulides & Orszag 2000) and to the pumping motion of the recirculating region, namely the $m = 0$ mode (Berger, Scholz & Schumm 1990). The azimuthal location of vortex shedding was determined by the orientation of the lateral force with respect to the x-axis. A time history of the azimuthal vortex shedding location is shown as a polar plot in figure 11(*b*), where time is the radius and the orientation of the force is the polar angle. A continuous rotation of the vortex shedding location would appear as a spiral emanating from the origin. The irregular rotation of the vortex shedding location can be observed in figure 11(*b*), where it randomly changes direction: it sometimes oscillates near an azimuthal location (around 30° in our case) and then suddenly makes a complete rotation around the circumference.

4. Conclusions

The transition process for a disk of aspect ratio 10, in the Reynolds number range of 10–300, was found to be a four-step process: (I) regular bifurcation; (II) Hopf bifurcation with three-dimensional flow and periodic rotation of the separation region; (III) periodic flow with planar symmetry and spatio-temporal symmetry; (IV) periodic three-dimensional flow with irregular rotation of the separation region. The regular bifurcation showed a double-threaded wake with planar symmetry, similar to that of the sphere. The second bifurcation to periodic shedding of double-sided hairpin vortices, resulted in a loss of the symmetry plane. The presence of double-sided vortices contrasts with the single-sided loops observed for a sphere. This vortex structure also caused the drag coefficient to oscillate at twice the frequency of the axial

velocity fluctuation. In the third bifurcation, the symmetry plane was recovered and the lift coefficient oscillated periodically with a zero mean, namely spatio-temporal symmetry. This transition process compares to that observed for an infinitely thin disk (Fabre, Auguste & Magnaudet 2007), indicating a threshold for the disk thickness beyond which the transition process is like that of a sphere. In the fourth step, irregular motion of the vortex shedding location was observed leading to the loss of the symmetry plane.

We plan to study the effect of disk aspect ratio on the transition process and also consider a moving disk.

We would like to thank the reviewers for their insightful comments. We acknowledge the use of ICEM-CFD and ANSYS-CFX10 (Ansys Inc., Canonsburg, PA) as part of the Ansys-CFPD Lab academic partnership.

REFERENCES

Achenbach, E. 1974 Vortex shedding from spheres. *J. Fluid Mech.* **62**, 209–221.

Barkley, D. & Henderson, R. D. 1996 Three-dimensional Floquet stability analysis of the wake of a circular cylinder. *J. Fluid Mech.* **322**, 215–241.

Barth, T. & Jespersen, D. 1989 The design and application of upwind schemes on unstructured meshes. *AIAA Paper* 89-0366.

Berger, E., Scholz, D. & Schumm, M. M. 1990 Coherent vortex structures in the wake of a sphere and a circular disk at rest and under forced vibrations. *J. Fluids Struct.* **4**, 231–257.

Brücker, C. 2001 Spatio-Temporal Reconstruction of vortex dynamics in axisymmetric wakes. *J. Fluids Struct.* **15**, 543–554.

Fabre, D., Auguste, F. & Magnaudet, J. 2007 Bifurcations and symmetry breakings in the wake of a disk. *Paper Presented at 60th Annual Meeting of the DFD, APS.*

Fernandes, P. C., Risso, F. R., Ern, P. & Magnaudet, J. 2007 Oscillatory motion and wake instability of freely rising axisymmetric bodies. *J. Fluid Mech.* **573**, 479–502.

Jeong, J. & Hussain, F. M. 1995 On the identification of a vortex. *J. Fluid Mech.* **285**, 69–94.

Johnson, T. A. & Patel, V. C. 1999 Flow past a sphere up to a reynolds number of 300. *J. Fluid Mech.* **378**, 19–70.

Magarvey, R. H. & Bishop, R. L. 1961 Transition ranges for three-dimensional wakes. *Can. J. Phys.* **39**, 1418–1422.

Marshall, D. & Stanton, T. E. 1930 On the eddy system in the wake of flat circular plates in three dimensional flow. *Proc. R. Soc. Lond.* A**130**, 295–301.

Mittal, R. 1999 Planar symmetry in the unsteady wake of a sphere. *AIAA J.* **37**, 388–390.

Natarajan, R. & Acrivos, A. 1993 The instability of the steady flow past spheres and disks. *J. Fluid Mech.* **254**, 323–344.

Ross, F. W. & Willmarth, W. W. 1971 Some experimental results on sphere and disk drag. *AIAA J.* **9**, 285–291.

Sakamoto, H. & Haniu, H. 1990 A study on vortex shedding from spheres in uniform flow. *Trans. ASME: J. Fluid Engng.* **112**, 386–392.

Thompson, M. C., Leweke, T. & Provansal, M. 2001 Kinematics and dynamics of sphere wake transition. *J. Fluids Struct.* **15**, 575–585.

Tomboulides, A. G. & Orszag, S. A. 2000 Numerical investigation of transitional and weak turbulent flow past a sphere. *J. Fluid Mech.* **416**, 45–73.